TECHNICAL PAPER

Improving Inner Quality in Continuous Casting Rectangular Billets: Comparison Between Mechanical Soft Reduction and Final Electromagnetic Stirring

Jie Zeng[1] · Weiqing Chen[1] · Qingxian Wang[2] · Guangshun Wang[2]

Abstract The comparison between the mechanical soft reduction (MSR) and final electromagnetic stirring (FEMS) on center carbon macrosegregation and v-segregation has been investigated in order to improve the inner quality of high carbon 82A steel with a section of size 180 mm × 240 mm. A heat transfer calculation model by using C++ programming language is developed and applied to calculate the appropriate casting speed of continuous casting during the FEMS and MSR processes. The calculated action zone of FEMS and MSR is at the location with a solid fraction of 0.28–0.41 and 0.30–0.90, respectively. The industrial results show that the effects of MSR in improving the center carbon segregation, reducing the shrinkage cavity and suppressing the V-segregation are more effective than FEMS. The mean center carbon segregation degree reduces from 1.19 to 1.15 with FEMS and decreases from 1.19 to 1.07 with MSR. Besides, compared with FEMS, MSR can eliminate shrinkage cavity and V-segregation but may generate center negative segregation and transverse cracks subjected to reduction pressure.

✉ Jie Zeng
zengjie2014@126.com

[1] State Key Laboratory of Advanced Metallurgy, University of Science and Technology Beijing, Beijing 100083, China

[2] Qingdao Iron and Steel Group Co., Ltd., Qingdao 266043, China

1 Introduction

As the demand for high grade steel increases, the improvement in control of inner quality such as centerline segregation and shrinkage cavity has become a major task in continuous casting. Among the solidification defects, center macrosegregation has been an especially serious problem for continuous casting of high-carbon steel billets and has a great influence on the final quality of wire rod [1–4]. Fundamental tasks of the high-carbon continuous casting are the optimization of processing parameters and reasonable use of continuous casting equipments to minimize the formation of carbon macrosegregation [5]. The centerline macrosegregation and shrinkage cavity are caused mainly by thermal contraction of the surrounding solidified shell as well as by solidification shrinkage of the final end of the liquid pool [6–8].

There have been various technologies to reduce the detrimental center carbon segregation in high-carbon continuous casting, such as low-temperature casting, mold electromagnetic stirring, thermal soft reduction, mechanical soft reduction, large reduction and final electromagnetic stirring [9–11]. Final electromagnetic stirring (FEMS) is industry standard on most billet casters producing critical steel grades especially high-carbon grades for wire rods and spring steels [12, 13]. To obtain optimum metallurgical benefits with FEMS, the stirrer and power supply are designed with variable frequency and operational current, both of which can be changed during operation. However, mechanical soft reduction technology has been used widely in continuous casting, especially found on slab and bloom casters with a sophisticated product mix [14, 15]. The principle of mechanical soft reduction is to impose an appropriate total reduction amount on a reasonable final solidification zone to suppress the formation of central

macrosegregation and porosity by compensating for the solidification shrinkage and preventing the suction flow of the residual melt [16, 17].

With FEMS, it is possible to achieve a homogeneous temperature field and give more equiaxed crystal at the residual liquid steel, and this usually decreases the center macrosegregation and porosity. With MSR, the center solidification shrinkage is compensated by the molten steel, and the solute-enriched liquid flowing toward to the center is prevented by the reduction force and, consequently, decreases the centerline macrosegregation and shrinkage cavity formation [18]. From the above analysis, it can be seen that both FEMS and MSR can improve the inner quality by decreasing the center macrosegregation and other solidification defects. However, the quantitative comparative results between FEMS and MSR is seldom investigated in the same steel grade and the same continuous casting. In addition, the industrial results will be helpful in choosing an appropriate way of achieving high-quality continuous billet.

The current work starts by developing a heat transfer calculation model by using C++ language which is applied to calculate the install location and appropriate casting speed during FEMS and MSR process. Then, an industrial test is conducted to investigate the effects of the two methods, FEMS and MSR, on the center macrosegregation, V-segregation and macro-defects such as the shrinkage cavity and center porosity in the rectangular billet continuous casting of 82A steel. Finally, the mechanisms and influences of FEMS and MSR on the inner quality of the rectangular billet are discussed.

2 Heat Transfer Model Description

In the present work, a 6-strand straight-arc rectangular billet continuous casting machine with a section size of 180 mm × 240 mm is researched, and its schematic is shown in Fig. 1. The FEMS is installed in the end of secondary cooling zone and the distance to the meniscus is 7.0 m. The MSR is carried out by five pair of withdrawal rolls, which are located between 10.77 and 13.91 m of the distance from the meniscus. As is well-known, finite difference method forms the basis of the numerical technique in the heat transfer calculation. By this method, an unsteady heat transfer model based on the "slice method" is developed to simulate the continuous casting process and to accurately calculate the appropriate casting speed. The slice unit moves down from the mold to the secondary cooling zone and finally to the air cooling zone. Each slice unit is tracked as it moves during continuous casting process. The control diagram is shown in Fig. 2.
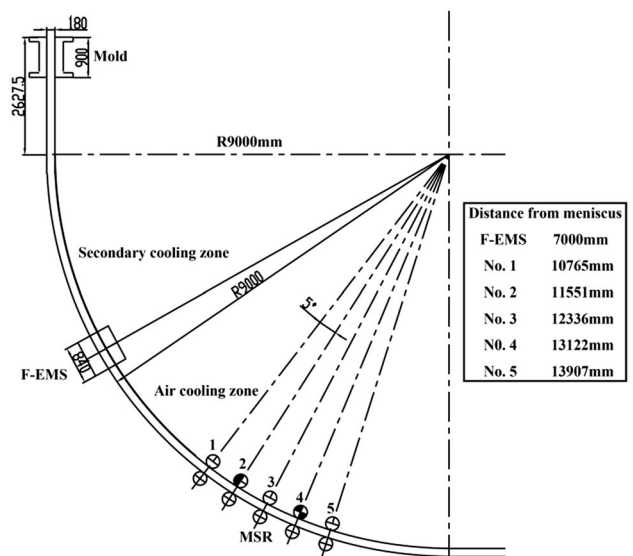

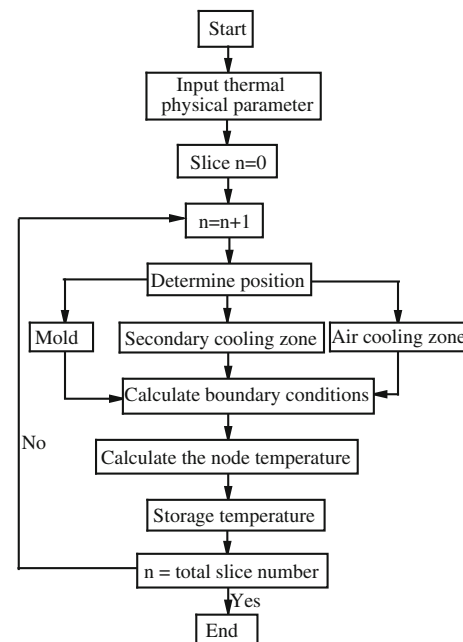Fig. 1 Schematic of rectangular billet continuous casting machine

Fig. 2 Flowchart of heat transfer calculation model

2.1 Model Formulation

2.1.1 Model Assumption

The main additional hypotheses employed in the calculation are as following:

(1) The density of solid and liquid phase is constant.
(2) The heat is only extracted in the transverse section of the billet.

(3) The latent heat of steel is converted into an effective specific heat in the mushy zone.

(4) The fluid flow is assumed to enhance heat transfer and then an effective thermal conductivity is employed in the liquid zone and mushy zone of billet [19].

2.1.2 Governing Equation

Based on the above simplified assumptions, the solidification process can be calculated by solving the Fourier's heat equation in two dimensions, as shown in Eq. (1). In the effective specific heat method, the evolution of the latent heat during the solidification has been incorporated into the calculation, such that both the sensible and latent heat of steel are included in the solidus and liquidus temperatures range, as shown in Eq. (2). The solid fraction is a key parameter in determining the mechanical soft reduction zone, as shown in Eq. (3).

$$\rho C_{eff} \frac{\partial T}{\partial t} = \frac{\partial}{\partial x}\left(k\frac{\partial T}{\partial x}\right) + \frac{\partial}{\partial y}\left(k\frac{\partial T}{\partial y}\right) \tag{1}$$

$$C_{eff} = \frac{C_S + C_L}{2} + \frac{L_f}{T_L - T_S} \tag{2}$$

$$f_s = \begin{cases} 0 & T \geq T_L \\ \dfrac{T_L - T}{T_L - T_S} & T_S < T < T_L \\ 1 & T \leq T_S \end{cases} \tag{3}$$

where ρ is the density, kg/m^3; C_{eff} is the effective specific heat, J/(kg °C); k is the thermal conductivity, W/(m K); T is the center temperature of the rectangular billet, °C; C_S is the specific heat capacity of solid steel, J/(kg °C); C_L is the specific heat capacity of liquid steel, J/(kg °C); L_f is the latent heat, J/kg; T_L is the liquidus temperature, °C; T_s is the solidus temperature, °C; f_s is the solid fraction.

2.1.3 Boundary Conditions

The boundary conditions including three sections namely the mold, secondary cooling zone and radiation zone, are given below. The extraction of heat from the surface of the billet proceeds by different mechanisms in each of the three cooling zones. The heat extraction processes are most complex in the mold and spray regions.

In the mold, heat transfer from the billet surface is influenced markedly by the formation of a gap between the mold and the solidifying steel shell. As the width of the gap appears to be very small, considerable heat can flow from the shell surface to the mold by conduction through the gas in the gap as well as by radiation. It is hard to describe the rate of heat flow because the gap width does not appear to be constant, but varies in both vertical and horizontal directions over the mold. In the

absence of mechanistic data of this kind, efforts have been made to obtain useful heat-flow data in the mold from a heat balance on the mold cooling water [20]. By this method, the average mold heat flux, q_m, can be obtained for a given set of casting conditions. The most important parameter that affects the mold heat flux q_m is the mold dwell time (equivalent to the distance below the meniscus). The heat flux in the mold is equalized to the empirical equation used by other workers, as shown in Eqs. (4)–(6) [21]. In Eq. (4), the coefficients a and b depend on the mold cooling condition. In the present work, the value of a is 2,680,000 and b can be calculated from Eqs. (5) and (6).

$$q_m = a - b\sqrt{L/v} \tag{4}$$

$$b = 1.5 \times (2680000 - \overline{q})/\sqrt{L_m/v} \tag{5}$$

$$\overline{q} = C_w \times w \times \Delta T /(S_{eff} \times 60) \tag{6}$$

where q_m is the heat flux of the mold, J/(m^2 s); L is the distance from the meniscus, m; v is the casting speed, m/min; L_m is the effective distance of the mold, m; C_w is the specific heat of the cooling water, J/(kg °C); w is the water flow rate in the mold, L/min; ΔT is the difference between the import and export temperature of the mold cooling water, °C; S_{eff} is the effective area of the mold wall, m^2.

In the secondary cooling zone, heat is removed from the billet by fast-moving water droplets which are ejected by a spray nozzle. These droplets penetrate the steam film adjacent to the steel surface and evaporate. Like the mold, this process is too complex to be treated theoretically. Instead, the rate of heat extraction, q_s, can be best characterized mathematically by a spray heat transfer coefficient, h_s [20]. By this method, the heat is removed from the surface and the heat flux is proportional to the heat transfer coefficient and the difference between the surface temperature and the temperature of the cooling water. The heat flux and the heat transfer coefficient in the secondary cooling zone can be expressed as Eqs. (7) to (8) [22]

$$q_s = h_s (T_b - T_w) \tag{7}$$

$$h_s = 200 + 10.44 W^{0.851} \tag{8}$$

where q_s is the heat flux of the secondary cooling zone, J/(m^2 s); h_s is the heat transfer coefficient of the secondary cooling zone, W/(m^2 °C); T_b is the surface temperature of the rectangular billet, °C; T_w is the temperature of the secondary cooling water, °C; W is the water flow rate of the secondary cooling zone, L/(m^2 min).

In the radiation zone, the heat extraction from the surface is given by the well-established Stefan–Boltzmann equation.

$$q = \varepsilon\sigma\left[(T_b + 273)^4 - (T_e + 273)^4\right] \tag{9}$$

where ε is the radiation coefficient; σ is the Stefan-Boltzmann constant, W/(m^2 K^4); T_b and T_e are the surface temperature of the rectangular billet and the environmental temperature of the air-cooling zone, respectively, K.

2.1.4 Initial Condition

The initial condition is given by Eq. (10):

$$T(x, y, z)_{t=0} = T_{pour} \tag{10}$$

where T_{pour} is the pouring temperature of steel, °C.

2.2 Material Properties

In order to obtain an accurate material properties of 82A steel between the solidus and liquidus temperatures range, the thermodynamic calculation softwares Thermo-Calc Windows (TCW) and CompuTherm LLC(from ProCAST software)are used in the research. The chemical compositions of the studied high carbon 82A steel are listed in Table 1. The main segregation element is carbon considering its high content and small solute distribution coefficient. The calculated material properties of 82A steel are shown in Fig. 3.

Figure 3a shows the variation of the solute segregation during the solidification process of 82A steel. Considering the diffusion of interstitial carbon in solid phase, the non-equilibrium solidification Scheil model is applied in the calculation. It can be seen from the figure that there are segregation of carbon element and the precipitation of MnS at final stage during solidification. The liquids temperature and solidus temperature are 1470 °C and 1353 °C, respectively.

The other material properties of 82A steel include the density, specific heat capacity and conductvity which are calculated based on the database from CompuTherm LLC, as shown in Fig. 3b–d. It can be seen from Fig. 3b that the density increases from 6900 to 7520 kg m^{-3} as the temperature decreases from 1500 to 1000 °C and the specific heat capacity has a transformation peak during solidification process. Besides, as the temperature decreases from 1500 to 800 °C, the thermal conductivity of 82A steel reduces from 34 to 26 W m^{-1} k^{-1}. The exact value of thermal conductivity has a significant influence on the solidification structure and the accurate thermo-physical properties calculation has a crucial influence on the

correctness of the solidification heat transfer calculation model. Based on the above calculation results, the main input parameters and constants used in solution of the model are shown in Table 2.

2.3 Model Validation

The validation of the heat transfer calculation model is performed by a comparison of the liquid core width and the surface temperature between the calculated and measured data. In order to determine the liquid core width at a distance of 9.73 m from the meniscus, the pin-shooting test is carried out on 82A steel at a casting speed of 1.0 m/min and secondary cooling water intensity of 0.9 L/kg, as shown in Fig. 4. As can be seen from Fig. 4, the width of the liquid core is about 25 mm. The calculated liquid core width from the heat transfer calculation model is 27.4 mm. The difference between the calculated and measured liquid core width is only 2.4 mm. Besides, six surface temperatures are measured using infrared pyrometer at a casting speed of 0.9 m/min and secondary cooling water intensity of 0.9 L/kg, as shown in Fig. 5. It shows fairly good agreement between the simulated temperatures and temperatures obtained from experiments and the surface temperature difference between the measured and calculated one is less than 27 °C. It can be concluded from the above validation analysis that the boundary conditions and materials properties are reasonable and the present model can be used to simulate the continuous casting process.

3 Test Parameters Calculation

The mechanical soft reduction zone is determined by calculating the distribution of solid fraction during the continuous casting. Thome and Harste [16] have shown that a reduction amount of 7–10 mm is necessary to ensure that a sufficient amount of reduction reaches the core to interrupt suction flow, and encouraging results are obtained for high-carbon steel at solid fraction between 0.2 and 0.9. Yim et al. [23] revealed that the optimum soft reduction is achieved when the solid fraction is between 0.2 and 0.8 and the total reduction amount is 7 mm in a bloom caster at Posco. Considering the above industrial results reported, the reduction zone is at the location with 0.3–0.9 in f_s and the total reduction amount is 8 mm in this research. There are a few papers reported in regard to the optimum stirring position of FEMS. The effect of FEMS on the decrease of macrosegregation is quite different depending on the stirring pool thickness and steel grade. The optimum stirring pool thickness at FEMS by plant tests is 55–65 mm for billet with a section size of 160 mm × 160 mm [12]. The stirring position of FEMS with a solid fraction of 0–0.4 is

Table 1 Chemical compositions of the 82A steel

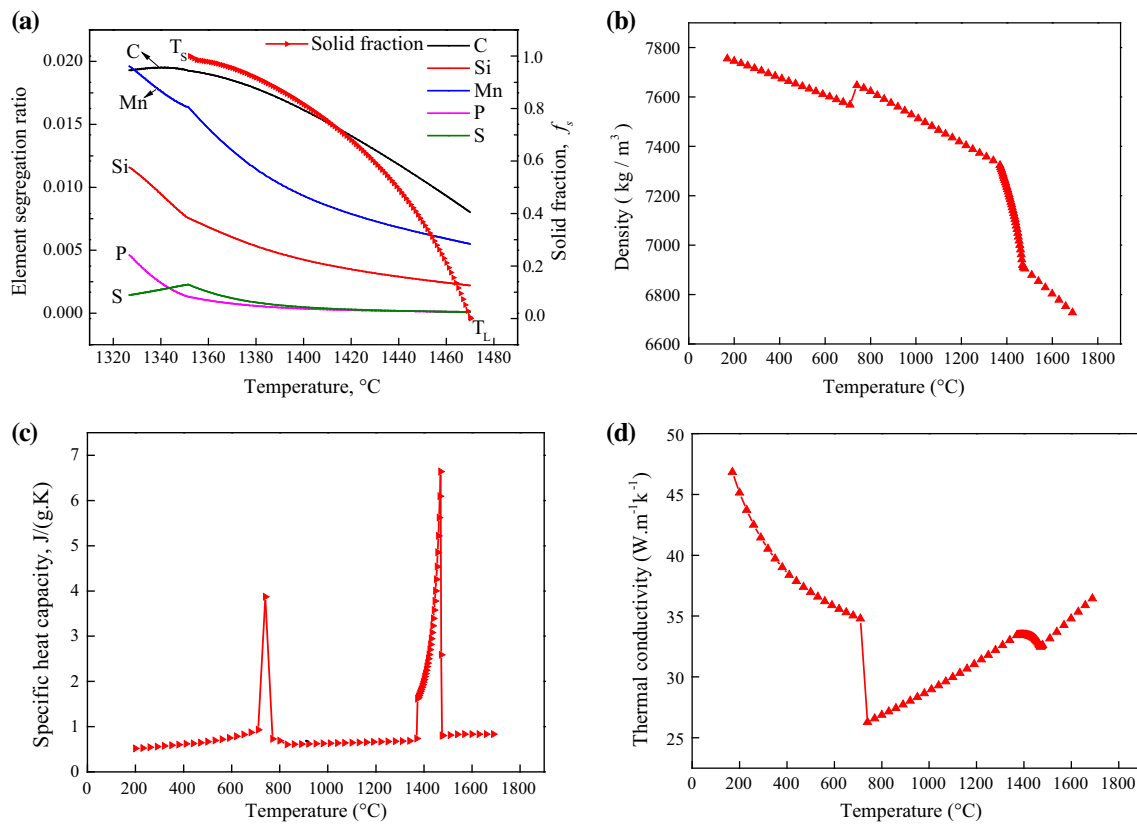| Composition	C	Si	Mn	P	S
Mass fraction (%)	0.82	0.20	0.55	0.014	0.007

Fig. 3 Solute segregation and material properties of 82A: **a** solute segregation and solid fraction; **b** density; **c** specific heat capacity; **d** thermal conductivity

Table 2 Main input parameters of 82A steel

Parameter	Value
Billet size (mm)	180×240
Effective mold length (mm)	800
Casting temperature (°C)	1495
Casting speed (m/min)	$0.8 \sim 1.4$
Secondary cooling water intensity (L/kg)	$0.4 \sim 1.0$
Density of liquid/solid steel (kg/m^3)	7000/7400
Liquid/Solidus temperature (°C)	1467/1366
Liquid/Solidus Specific heat capacity (J/(kg °C))	691/658
latent heat of steel (J/kg)	270,000
Water and ambient temperature difference (°C)	6

suitable to get more finer equiaxed crystal grains [24]. In this paper, the liquid thickness is set to 50–60 mm in the FEMS zone.

The final solidification position of the rectangular billet during continuous casting is calculated by using the heat transfer calculation model. The metallurgical lengths with different casting speeds and secondary cooling water intensities are shown in Fig. 6. The results shown in Fig. 6a demonstrate that the metallurgical length increases proportionately with the increasing casting speed from 0.8 to 1.4 m/min. As the casting speed increases by 0.1 m/min under the secondary cooling water intensity of 0.5 and 1.3 L/kg, the metallurgical length increases by 1.37 and 1.11 m, respectively. The metallurgical lengths with different secondary cooling water intensities are shown in Fig. 6b. The metallurgical length increases slowly with the secondary cooling water intensity decreasing from 1.0 to 0.4 L/kg. As the secondary cooling water intensity decreases by 0.1 m/min under the casting speed of 0.7 and 1.3 m/min, the metallurgical length only increases by 0.08 and 0.32 m, respectively. In this regard, compared with the changes of the secondary cooling water intensity, the variations of the casting speed have more effects on the total solidification time and metallurgical length.

As can be seen from Fig. 1, the FEMS is installed at the end of the secondary cooling zone and the distance to the meniscus is 7.0 m, and the MSR is located in the zone where the distance to the meniscus is 10.77–13.91 m. Considering the large distance between the FEMS and MSR, the industrial tests of FEMS and MSR have to consider different casting speeds. The appropriate casting speed can be calculated by the heat transfer calculation model.
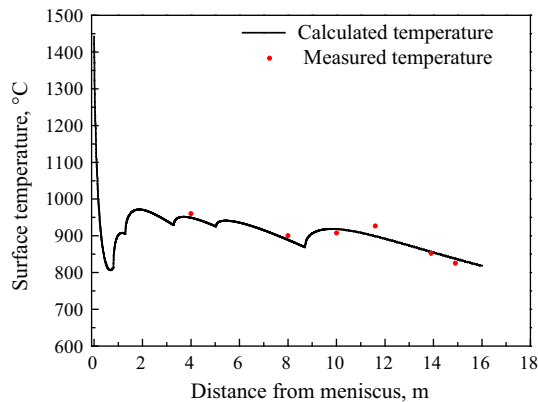
Fig. 4 Photo of pin-shooting

Fig. 5 Comparison of the measured and calculated surface temperature

In the secondary cooling water intensity of 0.9 L/kg, the effects of different casting speeds on the solid fraction and thickness of the residual liquid core are given in Fig. 7. It can be seen from Fig. 7a that the solid fraction changes as the casting speed increases from 0.8–1.4 m/min and the oblique line frame represents the appropriate soft reduction zone. The optimum casting speed of MSR is determined by investigating the length of the intersection line between the solidification curve and soft reduction zone. In this regard,

the solidification curve at a casting speed of 1.3 m/min has the longest intersection line and the casting speed can be selected as the optimum casting speed of MSR. Figure 7b illustrates the influences of different casting speeds on the thickness of the liquid core as the casting speeds varies from 0.8 to 1.4 m/min. The heavy line in Fig. 7b is used to indicate the optimum FEMS zone and only the liquid core curve with a casting speed of 0.9 m/min intersects the heavy line. So, the casting speed of 0.9 m/min is used as the appropriate test parameters of FEMS. Besides, the thickness of the liquid core is 50–60 mm and the corresponding solid fraction is 0.28–0.41 in the action zone of FEMS. In comparison to the MSR zone, the install position of FEMS is located in front of the MSR zone and the two techniques can be used simultaneously at an appropriate casting speed.

The 82A steel was produced by a straight curved caster with a section size of 180 mm × 240 mm. The secondary cooling water intensity was 0.9 L/kg and the superheat of the molten steel was about 25 °C. Test parameters for FEMS and MSR are presented in Table 3, where the stirring current and total reduction amount are 300A/6 Hz and 8 mm, respectively.

4 Industrial Results and Discussion

4.1 Center Carbon Segregation

The segregation degree is evaluated by drilling along the center line of the rectangular billet for every stirring parameter. Each sample is drilled out 4 mm in depth with a 5-mm diameter drill along the central longitudinal direction. The carbon segregation is defined as C/C_0, where C is the center carbon content (drilling test), C_0 is the carbon content in liquid steel (tundish test).

Compared to the manganese and phosphorus elements, the carbon centreline macrosegregation is the most serious problem for continuous casting of high-carbon steel. The

Fig. 6 The metallurgical length with different casting speeds (**a**) and secondary cooling water intensities (**b**)
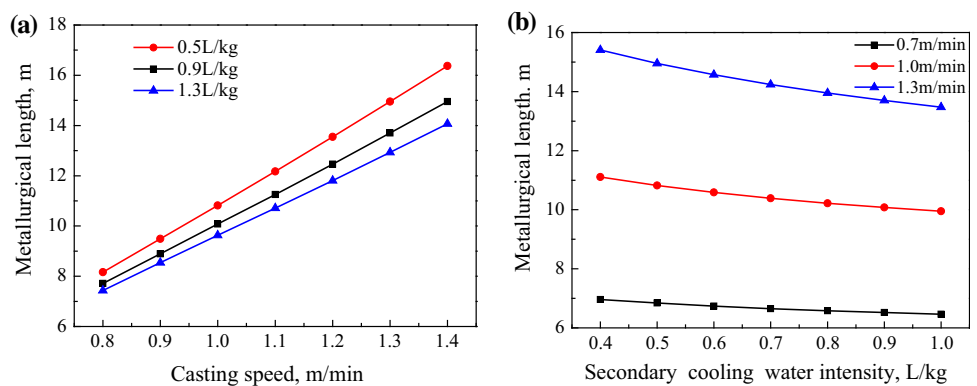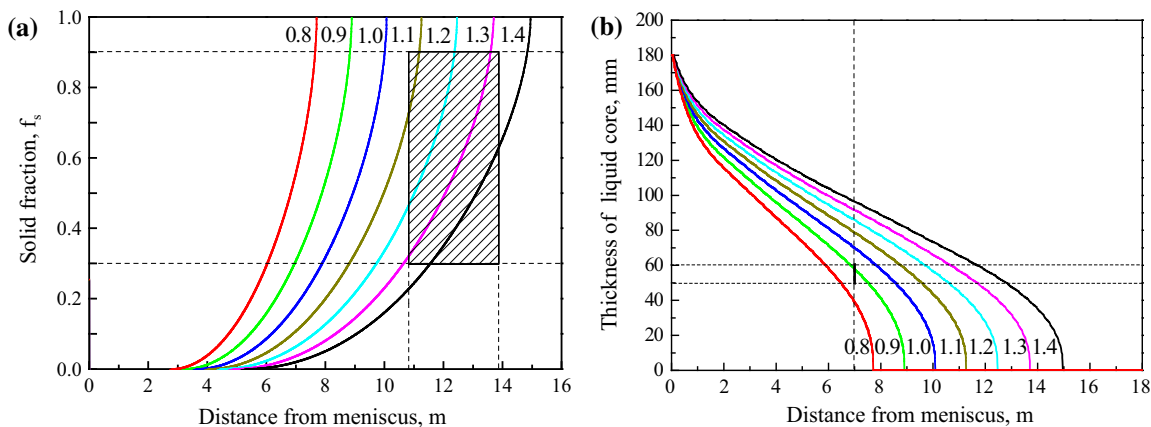
Fig. 7 Effects of different casting speeds on solid fraction (**a**) and thickness of residual liquid core (**b**)

Table 3 Test parameters of FEMS and MSR process

Test number	Control method	Casting speed (m/min)	Stirring current/ reduction amount	Strands no.
A	No-FEMS	0.9	0	1
B	FEMS	0.9	300 A/6 Hz	1
C	No-MSR	1.3	0	1
D	MSR	1.3	8 mm	1

central carbon segregation degree is calculated by ten drillings along the centreline under different conditions, as demonstrated in Fig. 8. The mean and maximum carbon segregation with No-FEMS and No-MSR processes are quite high though nearly the same. It can be seen that the casting speed of 1.3 or 0.9 m/min has little effect on the macrosegregation and the comparison of the two methods under different casting speed is feasible. The results as shown in Fig. 8a presents that the mean carbon segregation degree decreases from 1.19 to 1.15 and the maximum carbon segregation degree decreases from 1.27 to 1.20 with

the use of FEMS. A comparative assessment of the influence of MSR process on the center segregation degree is given in Fig. 8b. With MSR, the mean and maximum carbon segregation degree decreases from 1.19 to 1.07 and 1.23 to 1.15, respectively. In comparison to the FEMS, the application of MSR leads to a lower carbon segregation.

Although there are good results in segregation level in Fig. 8b. Further investigation of the centreline carbon segregation has shown that the MSR can lead to the center negative segregation. Figure 9 illustrates the carbon segregation degree at the centerline of the rectangular billet without and with MSR, respectively. The carbon segregation is obtained by total thirty drillings along the centerline of the rectangular billet. Although MSR leads to a lower segregation level in the center, the procedure produces 37 % center negative segregation in the rectangular billet. Due to the simultaneous compression of the strand core, the solute enriched liquid in the dendrite flowing to the center is prevented or the center residual liquid is discharged to the nearby dendrite. Essentially, the MSR process affects the flow direction of the residual molten liquid [25].
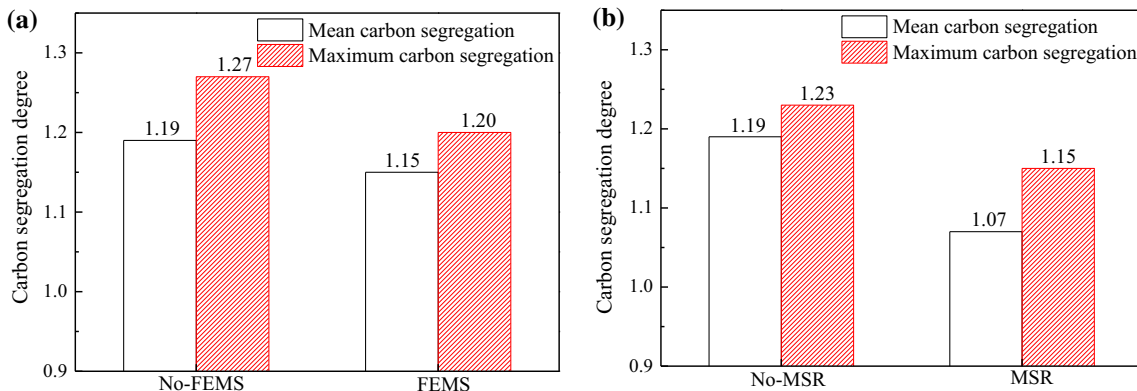

Fig. 8 Central carbon segregation degree of 82A steel: **a** without and with FEMS; **b** without and with MSR
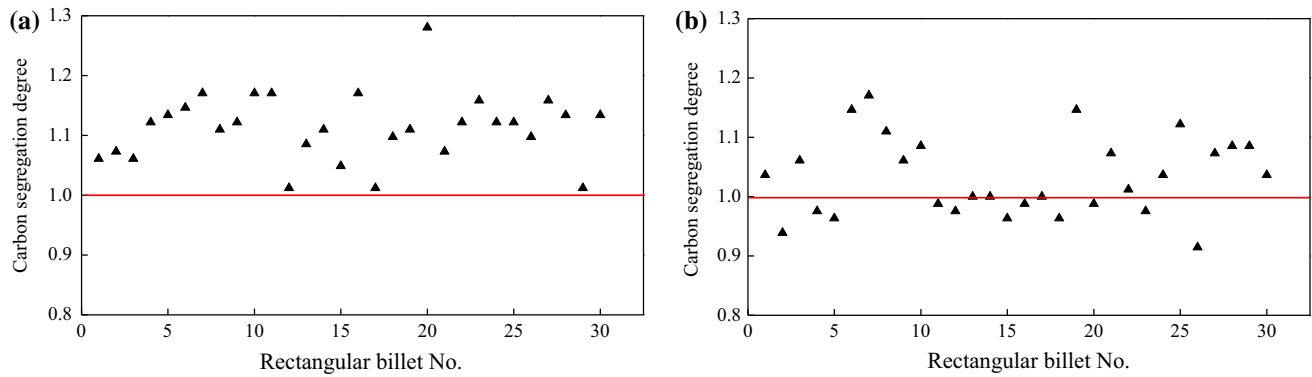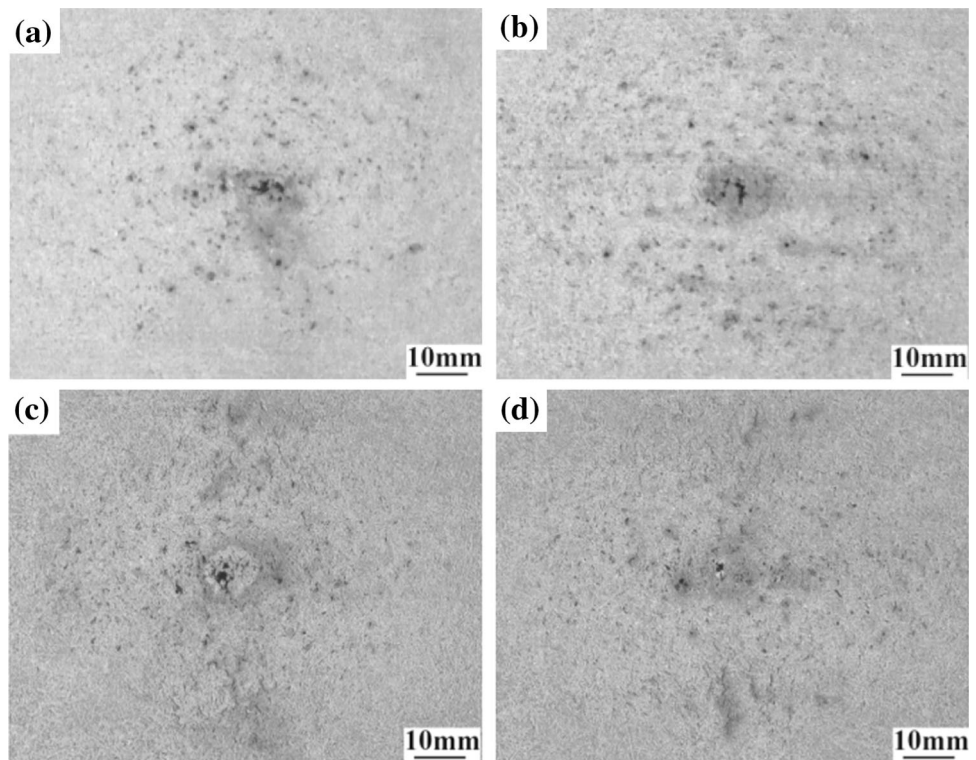
Fig. 9 The carbon segregation degree at the centerline of rectangular billet: **a** without and **b** with MSR

Fig. 10 Macrographs of center transverse section: **a** without and **b** with FEMS; **c** without and **d** with MSR

4.2 Macro-defects of Transverse Section

It is well known that the center porosity and shrinkage cavity occur in the center part of the continuous casting blooms or billets. The solidification macro-defects of the samples are revealed by using hydrochloric acid erosion method. Figure 10 illustrates the macrographs of center transverse section of 82A steel under different conditions. The images of the solidification structure without FEMS in Fig. 10a or without MSR in Fig. 10c clearly show that the central porosity and shrinkage cavity are apparent. The effects of FEMS on the central porosity and shrinkage cavity aren't such obvious, as shown in Fig. 10b. In

comparison to the macrographs with FEMS or without MSR, the central porosity and shrinkage cavity are less pronounced and more uniform in distribution with MSR, as shown in Fig. 10d.

4.3 Longitudinal Macrostructure and Microstructure

Figure 11 shows the macrographs of the center longitudinal section, which has been deeply etched with hydrochloric acid. The left image in Fig. 11 represents the case, in which the suppression of V-segregation and centerline shrinkage cavity is less distinct by FEMS. In comparison to the

Fig. 11 Macrographs of center longitudinal section: (*left*) FEMS and (*right*) MSR
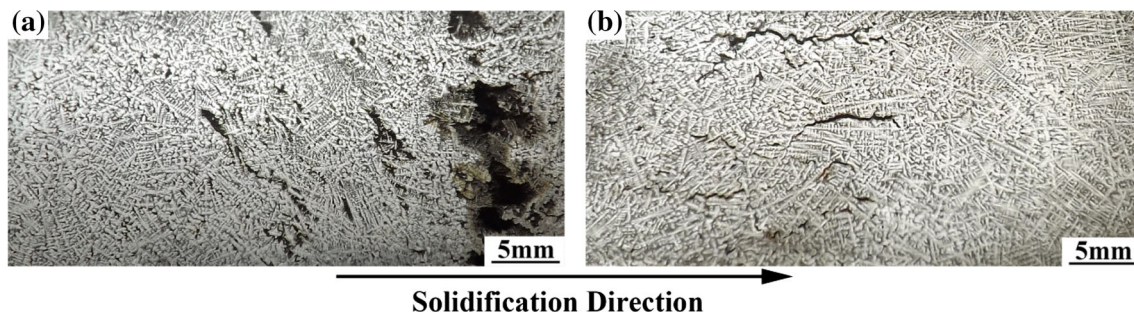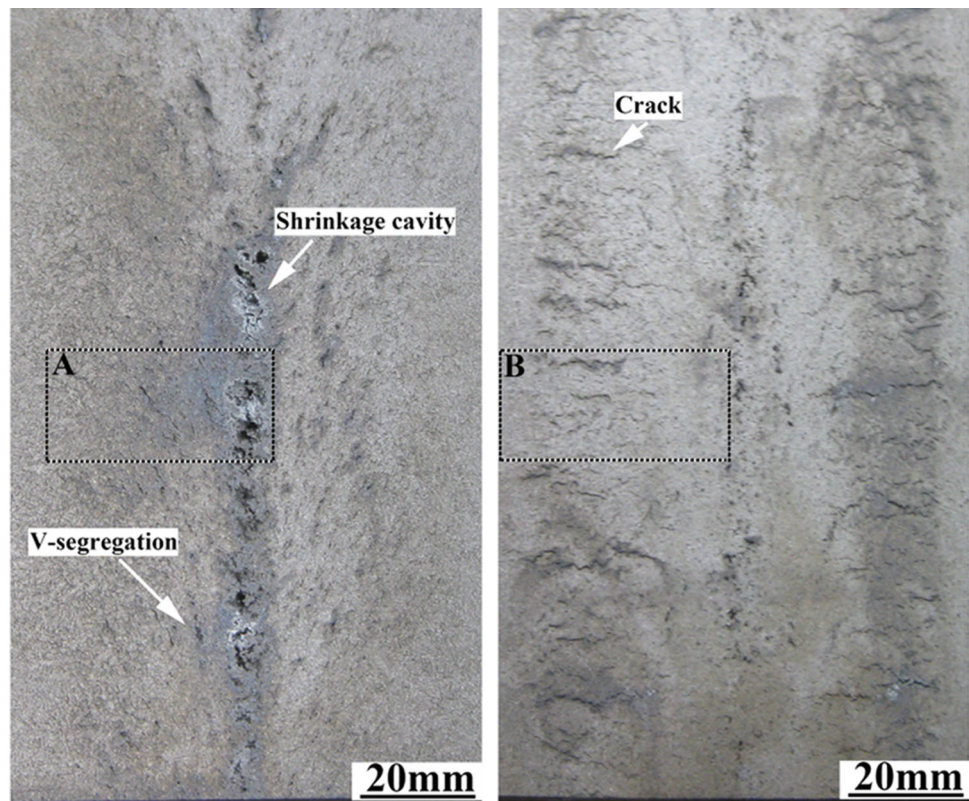

Fig. 12 Higher magnification view of solidification microstructure: **a** V-segregation channel and central shrinkage cavity and **b** interdendritic internal cracks

rectangular billet with FEMS, the formation of V-segregation in the central of rectangular billet subjected to MSR is suppressed and the centerline shrinkage cavity is clearly reduced as shown in the right image of Fig. 11. Although MSR suppresses the formation of V-segregation, the reduction process also produces clear internal cracks in the reduction zone with a length of about 20 mm and the internal cracks keep a distance of about 18 mm from the centerline. There are lot of reports about the generation of internal cracks on the applicability of MSR for billets, blooms and slabs [26, 27]. Decreasing V-segregation without producing internal cracks is only possible if the

reduction conditions are closely related to the material properties and the casting parameters [16].

In order to reveal the microstructure, samples have been etched with the following solution: Picric acid (60 g) + CuCl$_2$ (15 g) + liquid soap (60 cm^3) + water (3000 cm^3) [28]. Figure 12 illustrates a higher magnification view of the solidification microstructure and the sampling place of the specimen is shown by dotted squares marked as A and B in Fig. 11. Figure 12a shows the dendritic morphology of FEMS specimen with an apparent V-segregation channel and central shrinkage cavity. Highly enriched liquid flows from the interdendritic areas into the

center through the channel and causes the central macrosegregation. Figure 12b illustrates the influence of MSR on the dendrite morphology of center specimen. The interdendritic internal cracks are distinct and are located in the mushy zone with both columnar crystal and equiaxed crystal. The internal cracks are difficult to generate in the central zone containing fine equiaxed grains, because of the large crack propagation resistance. Besides, it can also be seen from Fig. 12 that the MSR has a significant effect on the dendrite morphology and a compact and uniform dendrite crystal is obtained. There is no obvious porosity in the center equiaxed dendrite zone compared with the dendrite morphology of billet with FEMS. So, the comparison reveals that the FEMS does not produce new internal cracks, but their center carbon segregation does not appears to be enough to satisfy customer's demand for best quality.

5 Conclusions

A heat transfer mathematical model has been developed to calculate the appropriate casting speed of FEMS and MSR process and an industrial plant trial has been conducted to investigate the influences of FEMS and MSR on the internal quality of 82A steel. The major findings resulting from numerical simulation and trials can be summarized as follows:

(1) Compared with the changes of secondary cooling water intensity, the variation of casting speed has a more effect on the metallurgical length which increases proportionately with the increasing of casting speed. The action zone of FEMS and MSR is at the location with a solid fraction of 0.28–0.41 and 0.30–0.90, respectively.

(2) Compared with FEMS, MSR is more effective to improve center segregation of the rectangular billet by suppressing the formation of V-segregation and decreasing the centerline shrinkage cavity and the disadvantages of MSR process are that, the center negative segregation and internal cracks are easy to generate.

(3) FEMS does not produce new internal cracks but their center segregation degree appears not to be enough to satisfy the demand for best quality. The FEMS and MSR maybe used together at an appropriate casting speed for the production of continuously cast steel that exhibits very low center macrosegregation and

the combination of the above two process needs further research.

References

1. Flemings M C, *ISIJ Int* **40** (2000) p 833.
2. Choudhary S K, and Ganguly S, *ISIJ Int* **47** (2007) p 1759.
3. Raihle C M, and Fredriksson H, *Metall Trans B* **25** (1994) p 123.
4. Sung P K, PoirierD R, Yalamanchili B, and Geiger G H,*Ironmak Steelmak* **17** (1990) p 424.
5. Ludlow V, Normanton A, Anderson A, Thiele M, Ciriza J, Laraudogoitia J, and Knoop W V, *Ironmak Steelmak* **32** (2005) p 68.
6. Fredriksson H, andSvensson I, *Metall Trans B* **7** (1976) p 599.
7. Engstrrm G, Fredriksson H, and Rogberg B, *Scand J Metall* **12** (1983) p 3.
8. Fredriksson H, *Can Metall Q* **30** (1991) p 235.
9. Raihle C M, Sivesson P, Tukiainen M, and Fredriksson H, *Ironmak Steelmak* **21** (1994) p 487.
10. Oh K S, Park J K, and Chang S H, *Steelmaking* in Conf Proc (1995) p 301.
11. Wang W J, Hu X G, Ning L X, Bulte R, and Bleck W, *Int J Miner Metall Mater* **13** (2006) p 490.
12. Oh K S, and Chang Y W, *ISIJ Int* **35** (1995) p 866.
13. Xiao C, Zhang J M, and Wu L, *J Iron Steel Res Int* **20** (2013) p 13.
14. Han Z W, Chen D F, Feng K, and Long M J, *ISIJ Int* **50** (2010) p 1637.
15. Sakaki G S, Kwong A T, and Petozzi J J, *Steelmaking* in Conf Proc (1995) p 295.
16. Thome R, and Harste K, *ISIJ Int* **46** (2006) p 1839.
17. Ogibayashi S, Kobayashi M, Yamada M, and Mukai T, *ISIJ Int.* **31** (1991) p 1400.
18. Ji C, Luo S, and Zhu M Y, *ISIJ Int* **54** (2014) p 504.
19. Thomas B G, and Zhang L, *ISIJ Int* **41** (2001) p 1181.
20. Brimacombe J K, *Can Metall Q* **15** (1976) p 163.
21. Choudhary S K, and Mazumdar D, *Steel Res Int* **66** (1995) pp 199.
22. Schwerdtfeger K J,*The Casting Volume of the 11th ed. of the Making, Shaping and Treating of Steel*, The AISE Steel Foundation, Pittsburgh (2003) p 18.
23. Yim C H , Park J K, Oh K S, and Nam S H, *Steelmaking* in Conf Proc (1998) p 309.
24. Mao B, Zhang G F, and Li A W, *Theory and Technology of Electromagnetic Stirring for Continuous Casting*, Metallurgical industry press, Beijing (2012) p 162.
25. Domitner J, Wu M, Kharicha A, Ludwig A, Kaufmann B, Reiter J, and Schaden T, *Metall Trans A* **45** (2014) p 1415.
26. Chen Y K, Feng F A, Lin K J, and Sediako D, *Steelmaking* in Conf Proc (1996) p 505.
27. Li X B , Ding H, Tang Z Y, and He J C, *Int J Miner Metall Mater* **19** (2012) p 21.
28. Cabrera-Marrero J M, Carreno-Galindo V, Morales R D, and Chavez-Alcala F, *ISIJ Int* **38** (1998) p 812.